

The effects of hydrogenation on the volatility of organic hydrogen getters.

H. N. Sharma, E. A. Sangalang, C. K. Saw, G. A. Cairns, C. D. Entwistle, W. McLean II, R. S. Maxwell, L. N. Dinh

March 20, 2017

Journal of Physical Chemistry

Disclaimer

This document was prepared as an account of work sponsored by an agency of the United States government. Neither the United States government nor Lawrence Livermore National Security, LLC, nor any of their employees makes any warranty, expressed or implied, or assumes any legal liability or responsibility for the accuracy, completeness, or usefulness of any information, apparatus, product, or process disclosed, or represents that its use would not infringe privately owned rights. Reference herein to any specific commercial product, process, or service by trade name, trademark, manufacturer, or otherwise does not necessarily constitute or imply its endorsement, recommendation, or favoring by the United States government or Lawrence Livermore National Security, LLC. The views and opinions of authors expressed herein do not necessarily state or reflect those of the United States government or Lawrence Livermore National Security, LLC, and shall not be used for advertising or product endorsement purposes.

Volatility of the catalytic hydrogenation products of 1,4 bis(phenylethynyl)benzene.

Hom N. Sharma¹, Elizabeth A. Sangalang¹, Cheng K. Saw¹, Gareth A. Cairns², William McLean¹, Robert S. Maxwell¹, and Long N. Dinh¹*

¹Lawrence Livermore National Laboratory, 7000 East Ave., Livermore, CA 94550 USA.

² AWE plc, Aldermaston, Reading, RG7 4PR, U.K.

*Corresponding author: dinh1@llnl.gov

KEYWORDS: Organic hydrogen getters, hydrogenation, equilibrium vapor pressures, meting temperatures, volatility.

ABSTRACT: Measurements of equilibrium vapor pressures by effusion thermogravimetry and melting points by differential scanning calorimetry (DSC) reveal that the melting temperature and equilibrium vapor pressures of 1,4-bis(phenylethynyl)benzene (DEB) do not vary monotonically with the hydrogenation extent. Contrary to intuition which suggests increasing volatility with hydrogenation, results indicate decreasing volatility for the first two hydrogenation steps before a non-monotonic upward trend, in which trans-isomers are less volatile. Insights on structural packing and functional groups were obtained from x-ray diffraction (XRD) and infrared (IR) studies to shed light on the observed variation in the volatility of DEB with hydrogenation. Density

functional theory (DFT) calculations were performed to obtain molecular level information and to establish the thermodynamics of DEB hydrogenation reactions. A major factor influencing the observed melting points and volatility of the hydrogenated intermediate species is identified as the local attractive or repulsive carbon-hydrogen (CH) dipole interactions among the getter molecules in their respective crystal structures. Such collective CH dipole interactions can be used to predict the trends in the volatilities of catalytic hydrogenation processes.

Introduction:

Solid state catalysis reactions are common for commercial industries such as food processing and bulk chemical production.[1-4] One particular application is the scavenging of excess hydrogen in sealed systems to prevent corrosion of nuclear materials, electronic components, and explosion hazards through the use of hydrogen "getters" compounded with a solid phase dispersed catalyst.[5-9] Due to their excellent hydrogen uptake capability and radiation resistance, poly-phenyl-ethynyl compounds are commonly used as hydrogen getters/scavengers while activated carbon with dispersed palladium (Pd) serves as catalytic support.[6, 8-12] These compounds chemically bind H₂ gas through hydrogenation reactions as opposed to physical surface adsorption.[5] The Pd catalyst dissociates molecular hydrogen into atomic hydrogen which then reacts directly with unsaturated bonds within migration distance of the atomic hydrogen. [6] Hydrogen scavenging by organic getters occurs in multiple steps, [13, 14] leading to the formation of various partially hydrogenated species. The performance of solid-phase catalytic systems at high temperatures and low pressures can be limited if the intermediate hydrogenated products have high volatilities. Under such conditions, the intermediates may migrate far from the reaction zone

of the catalytic surfaces and stop working prematurely, resulting in decreased performance and reduced uptake capacity.

Given the large difference in the melting points of 1,4-bis(phenylethynyl)benzene (DEB) and its fully hydrogenated version (452K and 360 K, respectively),[5] the measurements of the equilibrium vapor pressures and melting temperatures of intermediate hydrogenated species of DEB are needed to establish the volatility trend for DEB during the hydrogenation process. The knowledge on the evolution of the volatility of DEB in its scavenging life cycle serves as a model to understand the thermal behaviors of other organic getters and to determine the effective operational temperatures and environments.

In this work, the equilibrium vapor pressures, melting points, and structures of DEB from virgin state through fully hydrogenated state are probed by the Knudsen cell effusion technique, also known as effusion thermogravimetry, differential scanning calorimetry (DSC), x-ray diffraction (XRD), and Fourier Transform Infrared (FTIR). Density functional theory (DFT) calculations were used to estimate the relative thermodynamic stability of each species during hydrogenation reactions. Finally, collective CH dipole interactions in the structures of DEB species are proposed as a major factor in the observed trends for the measured melting points and equilibrium vapor pressures.

Materials and Methods

Getter material:

The molecular formula for DEB and the overall exothermic hydrogenation reaction is shown in figure 1.

Figure 1: A schematic of the overall reaction showing complete hydrogenation of a virgin DEB molecule.

In many applications, a mixture ratio of 75 % DEB and 25% catalyst (5% palladium on activated carbon) is exposed to environments containing a range of H₂ partial pressures.[15] The overall hydrogenation reaction is multistep and produces a range of intermediates. All the intermediates of DEB material studied here were provided by Johnson Matthey (UK) in the form of pure powder (>99% purity). Various analytical techniques such as nuclear magnetic resonance (NMR) and gas chromatograph mass spectrometry (GC-MS) were employed to verify the purities of the synthesized samples which were kept in sealed vials until experiments were performed. The nomenclature and structures of the investigated DEB samples are given in Table 1.

Table 1 The nomenclature and structures of the investigated DEB samples. Each DEB sample was named according to its hydrogen count and structural arrangement (e.g., T= trans, S= syn).

DEB material	Chemical name [16]	Molecular schematics
DEB	1,4-bis(phenylethynyl)benzene	
T2H-DEB	1-(Phenylethynyl)-4-(styryl)benzene	

T4H-DEB	1,4-distyrylbenzene	
S4H-DEB	1-(2-phenylethyl)-4- (phenylethynyl)benzene	
T6H-DEB	1-(2-Phenylethyl)-4-[(E)-2- phenylvinyl]benzene	
8H-DEB	1,4-bis(phenylethyl) benzene	

Experimental methods:

Knudsen cell effusion experiments:

The Knudsen effusion method involves placing a sample in a sealed container with a small orifice. The container is uniformly heated and held until equilibrium is attained between the condensed and vapor phases. In this study, custom built gold Knudsen cells with an average orifice diameter of ~ 0.05 mm were used. Each cell was placed in a thermogravimetric analyzer (TGA) and heated to the desired temperature in a vacuum level of $\sim 1 \times 10^{-5}$ Torr.

The equilibrium vapor pressure *P* can be computed as:[6]

$$P = \frac{1}{Af} \frac{dw}{dt} \sqrt{\frac{2\pi kT}{m}}$$
 [1]

where A, f, T, k, and m are the orifice area of Knudsen cell, Clausing factor, temperature, Boltzmann's constant and molecular mass, respectively. The Clausing factor is defined as

$$f = 1 - 0.5 \left(\frac{l}{r}\right) + 0.2 \left(\frac{l}{r}\right)^2$$
 [2]

where l and r are the Knudsen cell orifice length and radius. Equilibrium vapor pressures obtained at different temperatures are used to compute the enthalpy (ΔH_v) and entropy (ΔS_v) of vaporization as

$$\ln\left(\frac{P}{P_0}\right) = -\frac{\Delta H_v}{RT} + \frac{\Delta S_v}{R},\tag{3}$$

where P_o and R are the vapor pressure at the boiling point (1 atm) and molar gas constant, respectively. The slope of the linear plot of $\ln\left(\frac{P}{P_o}\right) vs. \frac{1}{T}$ yields ΔH_v while the intercept corresponds to ΔS_v .

DSC, XRD, and FTIR experiments:

Infrared (IR) spectroscopy experiments were carried out in the Diffuse Reflectance Infrared Fourier Transform Spectroscopy (DRIFT) mode. A polished gold surface was used to subtract the background signals. The scans were performed from 4000 to 400 nm wavelength.

DSC experiments to measure the melting point (T_m) of the DEB samples were conducted under flowing N₂. All samples were heated to a desired temperature (~573 K) with a constant heating rate of 5 K/minute.

XRD powder diffraction experiments were carried out with copper K_{α} radiation in the reflection mode along with sample spinning about the axis to randomize the crystal orientations during data acquisition. The generator was set at 40 KeV and 30 mA. Step scans were performed from 2 to 60 degrees (2 θ) with step size of 0.02 degree at 2 seconds per step.

Computational methods:

Density functional theory (DFT) calculations were performed using the Vienna ab initio simulation package (VASP)[17] and Gaussian09 software[18] packages. VASP calculations were performed using the generalized gradient approximation Perdew-Burke-Ernzerhof (PBE)[19]

functional for the exchange-correlation energies and using the projector augmented wave (PAW) frozen-core pseudo potentials. A plane wave energy cutoff of 500 eV was used for the plane-wave expansion of the wave functions. Gaussian09 calculations were performed with B3LYP[20, 21] DFT functional and the 6-31G(d) basis set.

The relative energy (ΔE) of each hydrogenation step was computed as:

$$\Delta E = E_{\text{DEB-species}} - E_{\text{virgin-DEB}} - nE_{\text{H}_2}$$
 [4]

where $E_{DEB-species}$, $E_{virgin-DEB}$, n, and E_{H_2} represent the energy of a specific DEB species, energy of virgin DEB (reference energy), number of hydrogen molecules, and energy of each hydrogen isolated molecule, respectively. The relative reaction energy for a hydrogenation step ($\Delta E_{rxn,i}$) was computed as:

$$\Delta E_{\text{rxn,i}} = \Delta E_{\text{step}_{(i)}} - \Delta E_{\text{step}_{(i-1)}}$$
 [5]

where ΔE_{step_i} and $\Delta E_{\text{step}_{(i-1)}}$ are the relative energy of a hydrogenation step *i* computed from Eq. 4, and the energy of previous hydrogenation step.

The dipole moment of the CH bonds in DEB species can be calculated once the atomic charge is obtained from the DFT calculation. The bond dipole moment was computed as:

$$\vec{\mu} = \sum_{i} q_i \vec{r_i} \tag{6}$$

where $\vec{\mu}$, q_i , and \vec{r}_i are the dipole moment vector, magnitude of i^{th} charge, and the vector representing the position of i^{th} charge. Here, the center of mass location was taken as the reference for distance calculations.

Results and Discussion

IR study:

DRIFT spectra of the DEB samples are shown in figure 2. The larger wavenumber region (\sim 3200–3000 cm⁻¹) corresponds to CH vibration mode, which provides a visual explanation of the hydrogenation of virgin DEB due to added CH bonds. In virgin DEB, sp^2 CH stretch IR peaks can be seen in the \sim 3200–3000 cm⁻¹ region.[22] With each hydrogenation step, new sp^2 CH bonds are added to the carbons between the phenyl rings. After 6 H atoms have been added to the virgin-DEB, an sp^3 CH stretch mode appears above 2800 cm⁻¹ region. IR peaks at \sim 2150 cm⁻¹ can only be seen in virgin DEB, which is due to the C \equiv C stretch of alkyne-type backbone of carbon connecting the phenyl rings. As expected, this peak disappears from other partially and fully hydrogenated DEB species. Aromatic C=C stretching peaks, present in all DEB species, appear at the \sim 1600-1500 cm^{-1} region. A band of IR peaks in the low wavenumber region is due to CH out-of-plane bending and in-plane bending, which occurs at \sim 900-690 cm⁻¹ and \sim 1275-1000 cm⁻¹ regions, respectively.

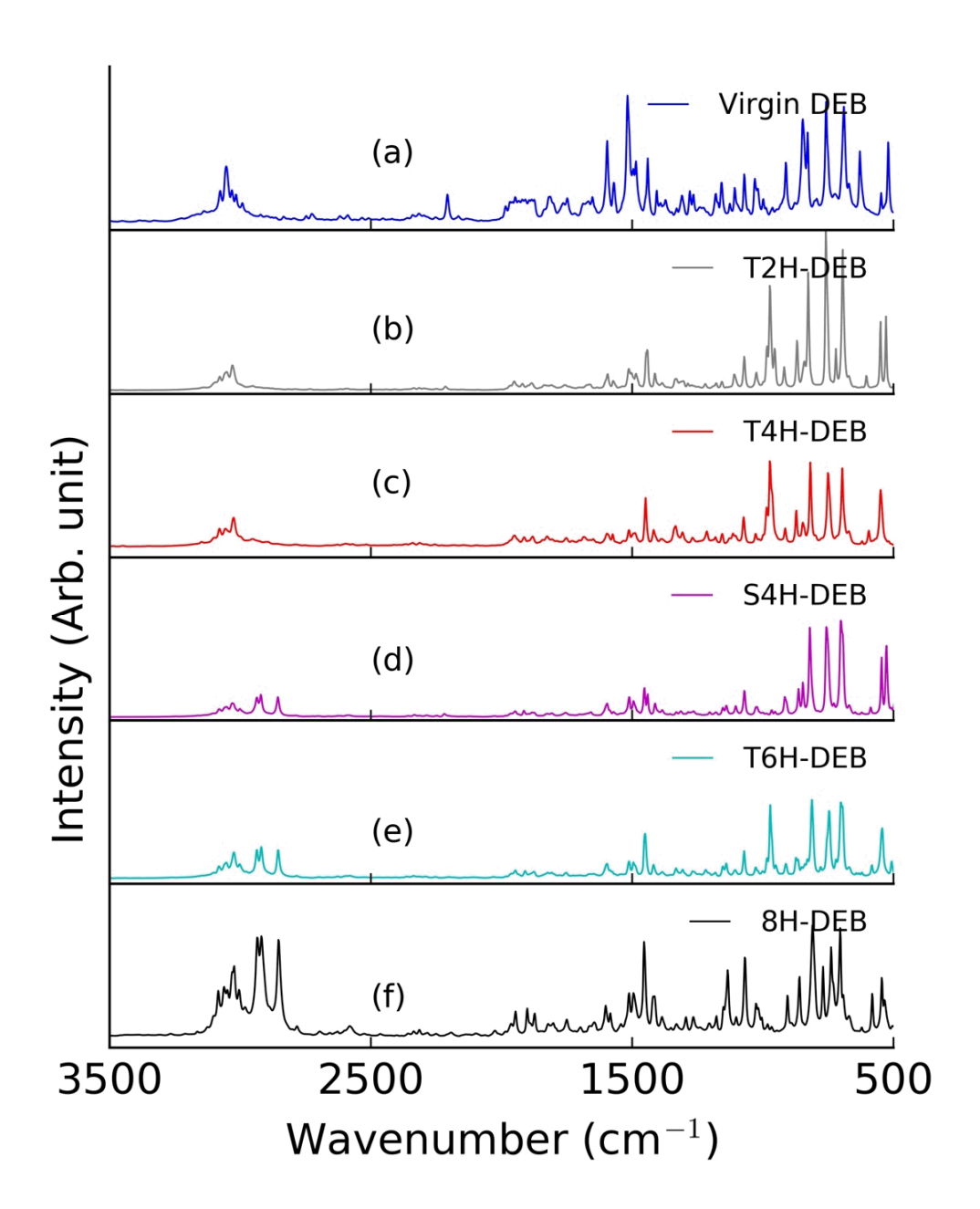


Figure 2: DRIFT spectra for the different DEB species.

Equilibrium vapor pressures:

The measured equilibrium vapor pressures for various DEB species are presented in the semi-log plot of log(equilibrium vapor pressure) vs 1/T in figure 3. The least volatile species is

T4H-DEB (a trans isomer), which exhibits the lowest equilibrium vapor pressures at all temperatures (e.g., 1.93×10^{-5} Torr at 383 K and 7.07×10^{-4} Torr at 423 K). The fully hydrogenated species, 8H-DEB, was found to be the most volatile species (1.88×10^{-5} torr at 323 K and 2.1×10^{-1} Torr at 398 K). The enthalpies, entropies, and room temperature (300K) equilibrium vapor pressures corresponding to each DEB species were obtained with Eq. 3 and are listed in Table 2. The entropy of vaporization (ΔS_v) quantifies the level of disorder in the system and is seen to increase with the following order: T4H-DEB, T2H-DEB, T6H, virgin DEB, S4H-DEB, and 8H-DEB. There is not a monotonic trend for the equilibrium vapor pressures with respect to hydrogenation level. T4H-DEB and T2H-DEB have lower while T6H-DEB has higher equilibrium vapor pressures than virgin DEB does. The syn species, S4H-DEB has significantly higher equilibrium vapor pressure than its counterpart, the trans isomer T4H-DEB.

On the practical level, despite the variation in the volatility of DEB during the hydrogenation process, the equilibrium vapor pressure of the most volatile hydrogenated product (8H-DEB) is in the 10⁻⁵ Torr range at 323K. This suggests that DEB is a suitable hydrogen getter for gas-filled and low vacuum applications with operational temperature below 323K.

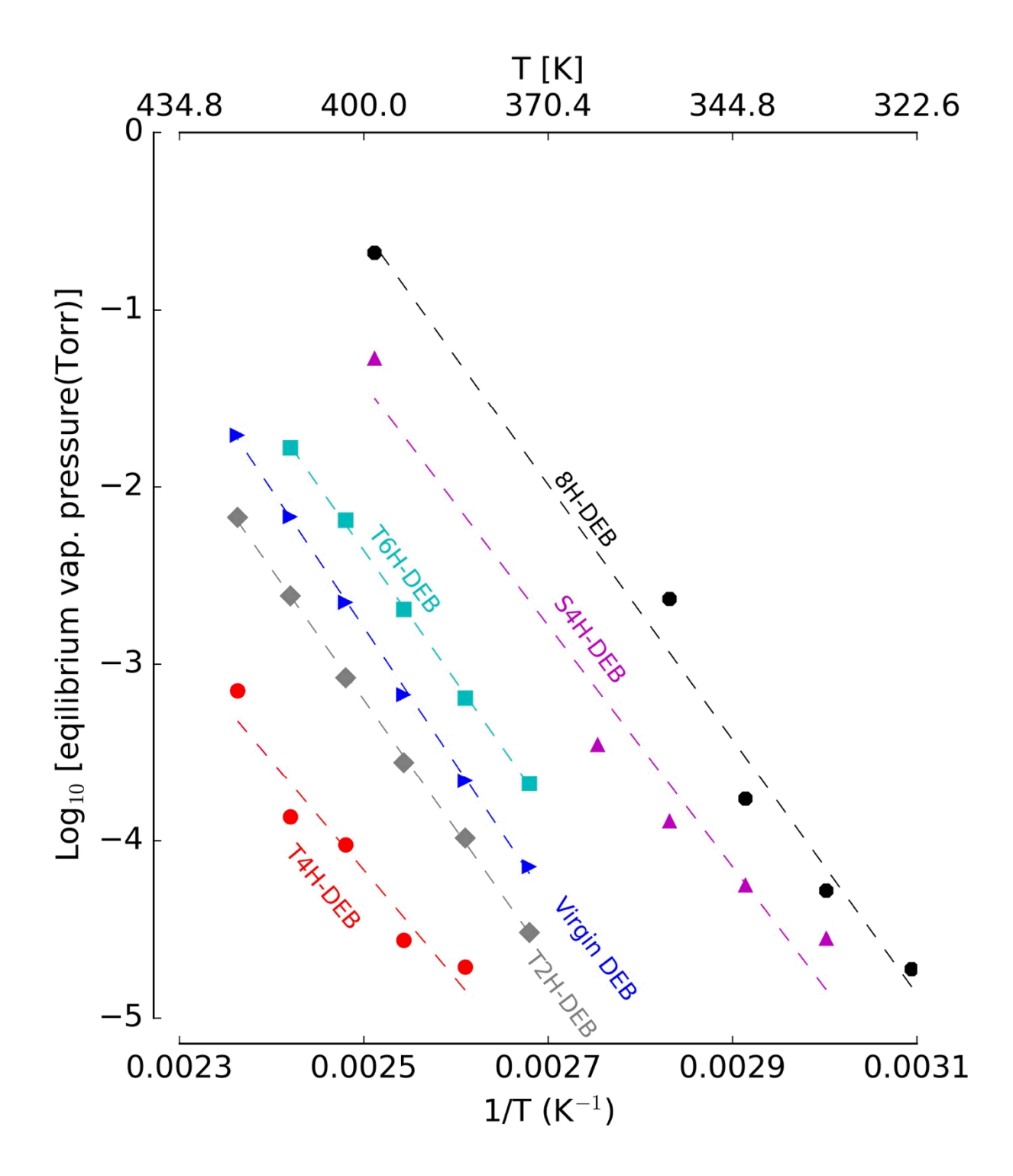


Figure 3: Equilibrium vapor pressure of DPB species at various temperatures. Symbols correspond to experimental data points and dotted lines are linear fits to guide the eyes.

Table 2: Computed equilibrium vapor pressures at 300K, enthalpies (ΔH_v) and entropies (ΔS_v) of vaporization of DEB species.

Sample	ΔH_v	ΔS_v	Equilibrium vapor pressure
	(J/mol)	(J/mol K)	at 300K
			(Torr)
Virgin DEB	-1.48×10^5	262.2	5.6×10^{-10}
T2H-DEB	-1.40×10^{5}	235.8	4.9×10^{-10}
T4H-DEB	-1.80×10^{5}	160.2	4.6×10^{-10}
S4H-DEB	-1.52×10^5	271.8	7.9×10^{-8}
T6H-DEB	-1.41×10^{5}	253.5	3.0×10^{-9}
8H-DEB	-1.37×10^5	278.5	2.8×10^{-7}

Melting temperatures:

Figure 4 shows the measured DSC curves. The presence of exotherm (negative heat flow behavior) in figure 4 indicates melting of the DEB species. The highest melting point, 538 K, was observed for T4H-DEB whereas the lowest melting point, 366.2 K, was observed for 8H-DEB. The DEB melting points observed in this DSC study are in close agreement with other experimental results for virgin DEB, T2H-DEB, T4H-DEB, and fully hydrogenated DEB species. [16] The smaller peaks at lower temperatures than the melting points in the DSC curves for 8H-DEB, T4H-DEB, and virgin DEB are most probably due to eutectic impurities in those samples.

The melting points for the DEB species are observed to correlate inversely with the measured equilibrium vapor pressures (i.e., species with high meting temperatures have low equilibrium vapor pressures) as seen in figure 5.

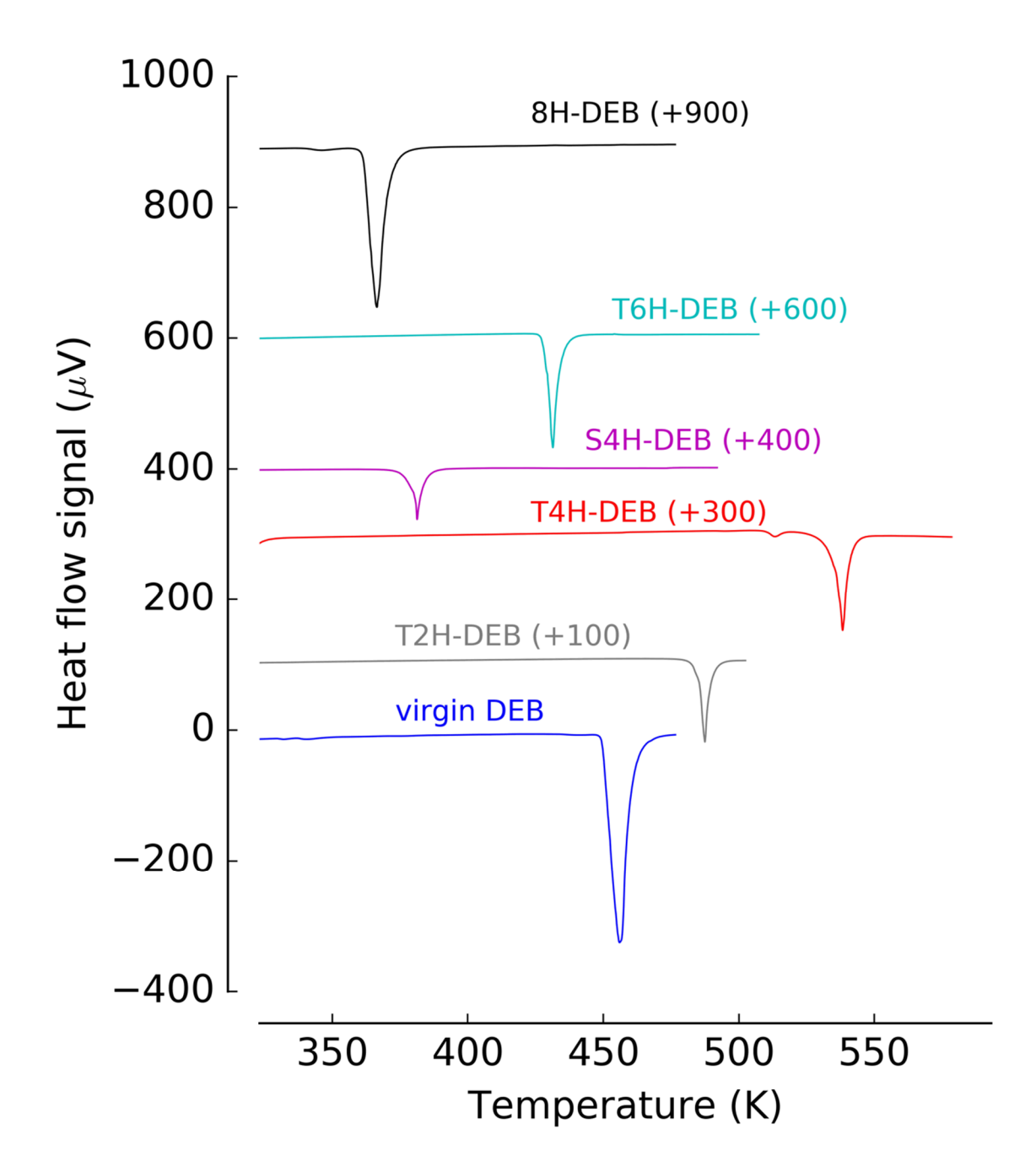


Figure 4: Heat flow signals (in μV) from DEB species during DSC experiments. The heating rate was 5 K/minute for all experiments. The negative peak in each curve represents the melting point of the corresponding species. The smaller peaks at lower temperatures than the melting points in the DSC curves for 8H-DEB, T4H-DEB, and virgin DEB are most probably due to eutectic impurities. Numbers shown in the bracket next to the DEB intermediates represent the vertical offset added to the actual heat flow signal.

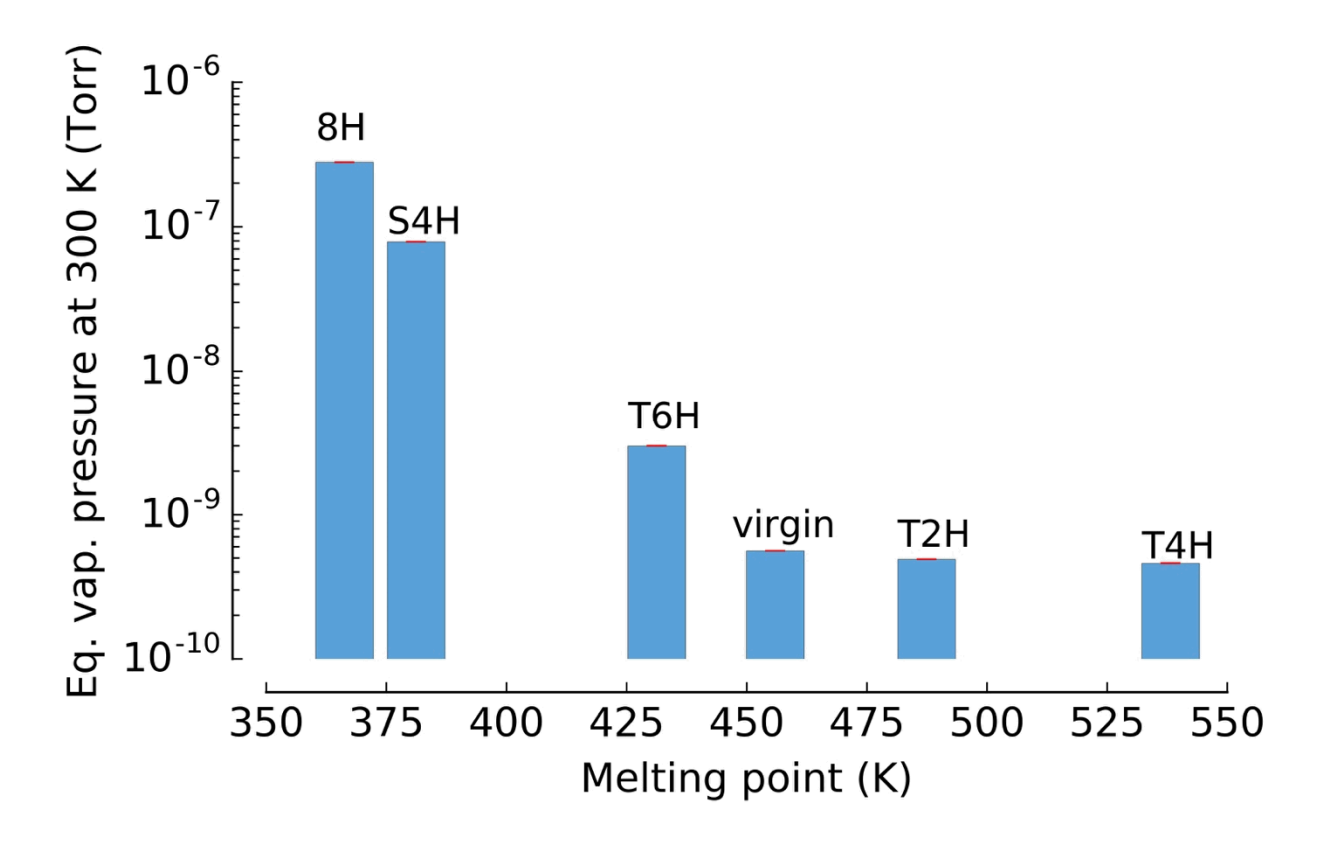


Figure 5: Bar plot showing equilibrium vapor pressure (in Torr) at 300 K vs melting point comparison for various DEB samples. T4H DEB, with the highest melting point temperature, shows the lowest equilibrium vapor pressure at room temperature.

XRD investigation:

The crystal packing structures of various DEB species as obtained from XRD are shown in figure 6. Left panels (a-f) plot intensities vs 2θ and right panels (g-l) show intensities vs stacking distances (d-spacing) of various crystal planes in the DEB samples.

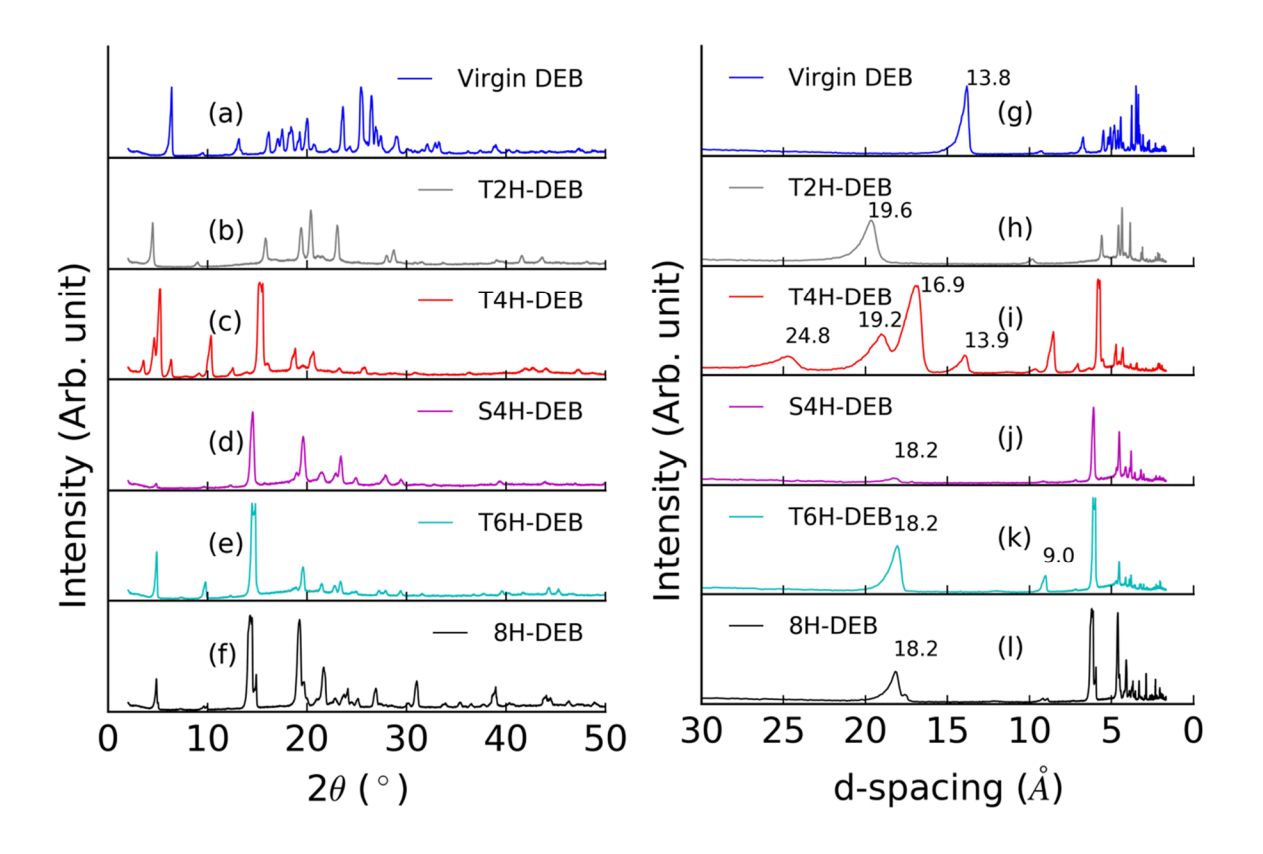


Figure 6: XRD analysis of DEB species. Panels (a-f): Intensities vs 2θ (left panels), and panels (g-l): intensities vs d-spacing plots (right panels). DEB getter names are shown next to the XRD curve in each panel.

To our knowledge, there is no information on the crystal packing structures for most of these DEB species except for virgin-DEB and T4H-DEB (discussed later). The molecular structures are also complex due to the large number of atoms. Hence, a direct comparison of peaks

to the crystallographic planes is not considered here. Instead, d-stacking distances are used to explain the orientation of benzene rings in DEB and its hydrogenated products. Analysis shows the presence of three main types[23] of aromatic ring configurations in DEB samples (see figure 7). The first one is the 'sandwich type' with phenyl rings stacked directly on top of one another. T2H-DEB displays this kind of interaction along with other DEB intermediates. The second one, most commonly found among all the DEB species considered in this report, is the 'T-shaped type' configuration, where one ring is at a right angle to another. The final type is 'parallel-displaced', as seen in T4H-DEB, where a phenyl ring is placed on top of another but displaced by some distance.

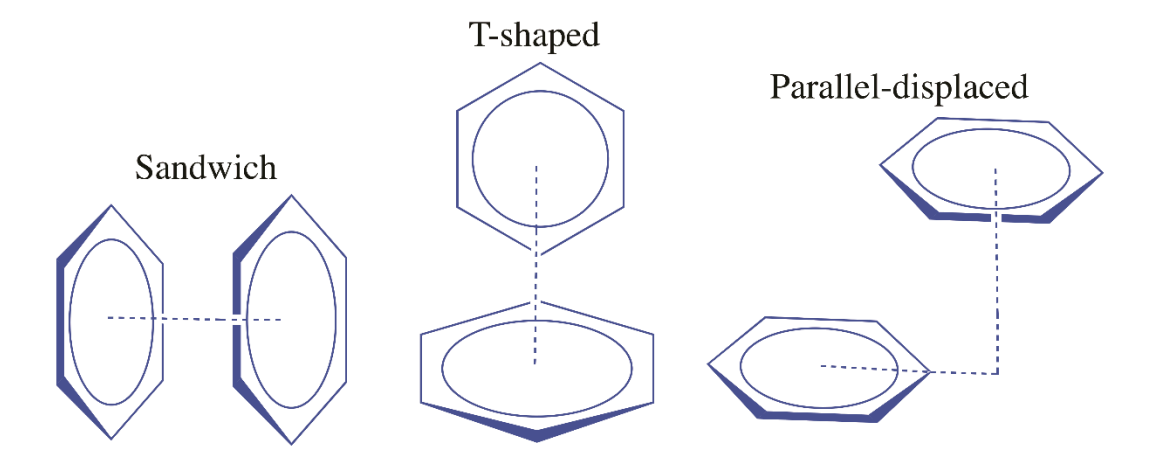


Figure 7: Schematics of phenyl ring (aromatic ring) configurations evident in DEB bulk crystal structures from XRD analysis.

Phenyl ring configurations are typically governed by ' $\pi - \pi$ ' interactions (attractive non-covalent interaction). For instance, the benzene dimer in gas phase is bound by T- shaped type ring configuration with relatively weak (~2 kcal/mol) energy and with a separation of rings by 4.96 Å. [23] In the absence of dipole interactions in benzene type (only with rings), quadrupole interactions becomes more relevant. [24] The appearance of XRD peaks at low angles can be correlated to the

ordering of the highest electron density regions (arising from the parallel stacking up of the phenyl rings). Typically, a 2θ of $\sim 9^{\circ}$ or below and d-spacing of ~ 9 Å or above are associated with the intermolecular spacings/interactions. Several peaks with d-stacking distances ≥ 9 Å (e.g., ~9 Å, ~14 Å, ~16.9, ~18 Å, ~19.6 Å, and ~25 Å) were observed from the XRD analysis (see figure 6, panels g-l). Since the T-shaped stacking has ~ 4.5 Å spacing, the 9 Å can be correlated to the reversed T-shaped configuration (T-reversed T). The 18 Å peak is possibly the 2nd order x-ray peak for this configuration and can be observed in 8H-DEB, S4H-DEB and T6H-DEB. Differences in peak intensities are most likely due to different amounts of ordering. For the virgin DEB where there are no hydrogen atoms attached to the back-bone carbons to interfere with the phenyl-phenyl rings stacking, 3-T-shaped configuration (T-reversed T and T) can be formed. Essentially, this is just an extra "T" added to the T-reversed "T". This is consistent with the 14 Å order and is also strongly present in T4H-DEB, but not in T2H-DEB, T6H-DEB, or S4H-DEB. Multiple peaks in the intermolecular spacing (d-spacing) of T4H-DEB are indicative of its highly-ordered structure. The additional d-spacing peaks for T4H-DEB are due to either the sandwich or parallel displaced configurations. This enhanced long range stacking order correlates well with the highest melting temperature observed for T4H-DEB. Unfortunately, due to the fixed number aromatic phenyl rings in all DEB species, the quadrupole interactions as evaluated by XRD remain approximately on the same order of magnitude, and, therefore, cannot be the deciding factor in the measured melting temperatures of partially hydrogenated DEB species.

Collective CH Dipole Interactions:

DEB species (with exclusion of virgin-DEB) have CH bonds that can exhibit localized bond dipoles. Schematics to show such CH bond dipole interactions in each pair of virgin DEB,

T4H-DEB, and 8H-DEB are shown in figure 8. The local CH dipole interactions may be relatively weak, but collective dipole interactions among adjacent molecules in a whole crystal can have a significant effect on both the melting temperatures and hence equilibrium vapor pressures of the DEB species. In Table 3, the type and number of possible CH dipole interactions are given. Attractive dipole interaction ("+" sign in Table 3) are present when opposite charges of the dipoles from two adjacent molecules line up as in T4H-DEB (figure 8 (b)). T4H-DEB has a total 8 attractive CH dipole interactions (4 positively charged H atoms and 4 negatively charged C atoms of a T4H-DEB interact attractively with 4 negatively charged C atoms and 4 positively charged H atoms of the two neighboring molecules, respectively). Analogously, repulsive dipole interactions ("-" sign in Table 3) are present when dipoles of similar charges from two adjacent molecules line up as in 8H-DEB (figure 8 (c)). From the column of "Net possible CH dipole interactions" in Table 3, it is seen that the crystal structures with the highest melting points have the highest number of attractive dipole interactions per molecule, while the crystal structures with the lowest melting points have the highest number of repulsive dipole interactions per molecule.

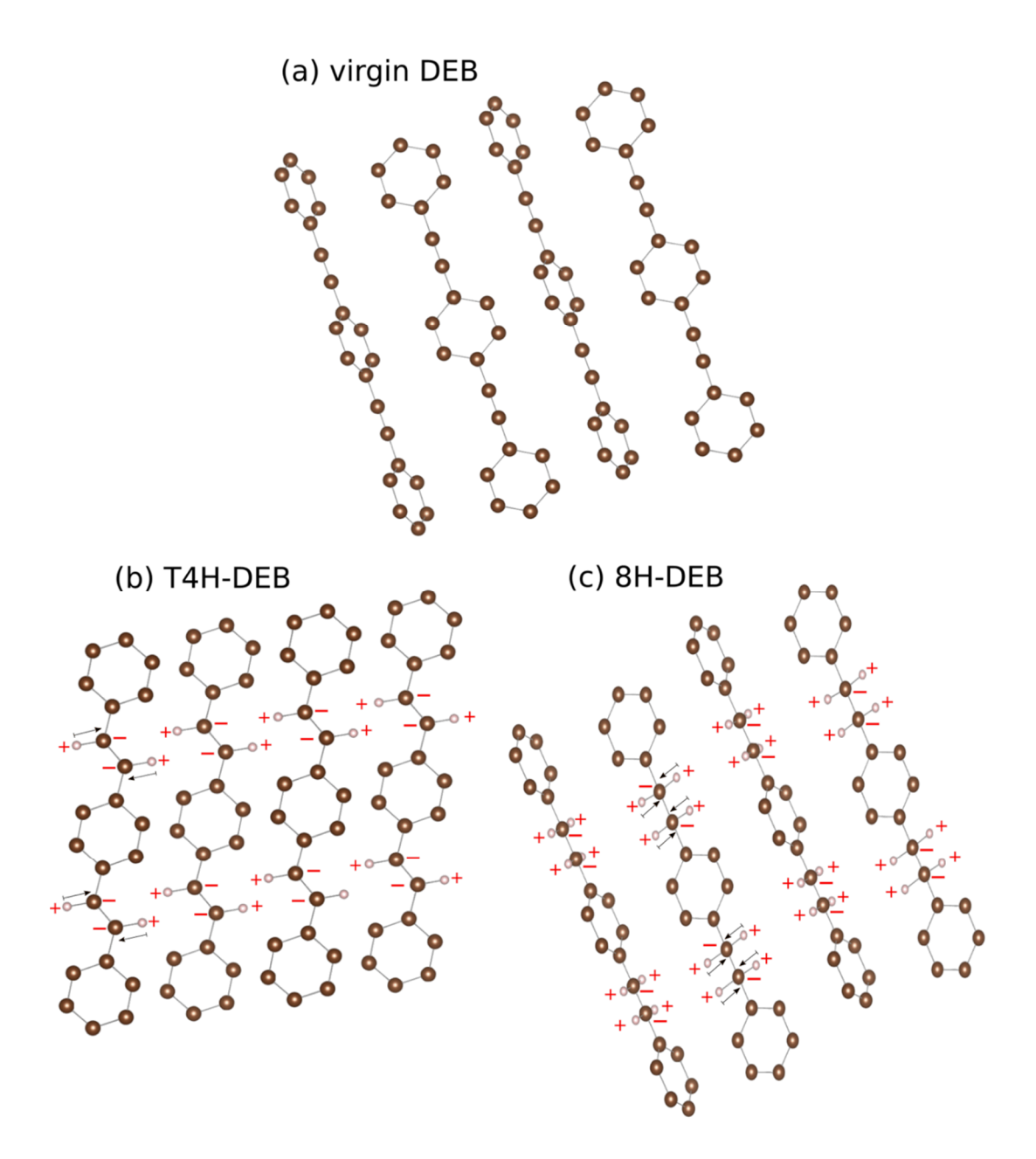


Figure 8: Schematics (2D projection of 3D structure) of (a) virgin DEB, (b) T4H-DEB, and (c) 8H-DEB showing the possibility of CH bond dipole interactions. Virgin DEB, T4H-DEB, and 8H-DEB have 0, 8 attractive, and 8 repulsive CH bond dipole interactions per molecule, respectively. Positive (+) and negative (-) charge centers are shown in T4H-DEB and 8H-DEB molecules. The H atoms in the benzene rings is not shown. The C-C bonds in the backbone of virgin DEB are triple bonds while those in T4H-DEB are double bonds (actual bonds are not shown).

Table 3: Types of aromatic ring stacking and possible CH dipole interactions in DEB species. Melting points given in this table are from DSC experiments as shown in figure 4.

Sample	T _m (K)	Aromatic-ring configuration	Net possible CH dipole interactions	
Virgin DEB	455.9	T-shape	0	
T2H-DEB	487.4	T-shape, Parallel or sandwich	4	
T4H-DEB	538.2	-	8	
		T-shape, parallel, offset stacking	-	
S4H-DEB	381.2	T-shape	-4	
T6H-DEB	431.3	T-shape	0	
8H-DEB	366.3	T-shape	-8	

Certainly, other factors such as structural complexity, quadrupole moments, varying bond order, charge distribution, and packing alignment all have certain effects on the overall volatility of each DEB species. Nonetheless, collective CH bond dipole interactions in the hydrogenated DEB crystal structures correspond well with the results from equilibrium vapor pressure and melting point measurements, and, therefore, play a significant role in the overall volatility of the DEB series.

Theoretical Calculations

Theoretical investigation of atomic charges, total energy, and IR modes for the DEB species (gas and crystal phases) were conducted to acquire molecular level information. Crystallographic information was available only for virgin-DEB and T4H-DEB, thus, crystal state computations were limited to those species only.

Computational results:

Figure 9 shows the optimized gas phase structures of the various intermediates of DEB during the hydrogenation process. The 2H, 4H, and 6H hydrogenated species exhibit more than one isomer as shown in figure 9. In general, *trans* species (except for T6H-DEB) are found to be linear whereas the *cis* isomers exhibit non-linear shapes. Linear structures in *trans* isomers with 2H and 4H can be packed more densely and are expected to show net attractive CH dipole-dipole interactions within the crystal. Denser packing (usually associated with stronger intermolecular attractions) and a net attractive dipole-dipole interaction in these trans isomer crystal structures should lead to higher melting temperatures.

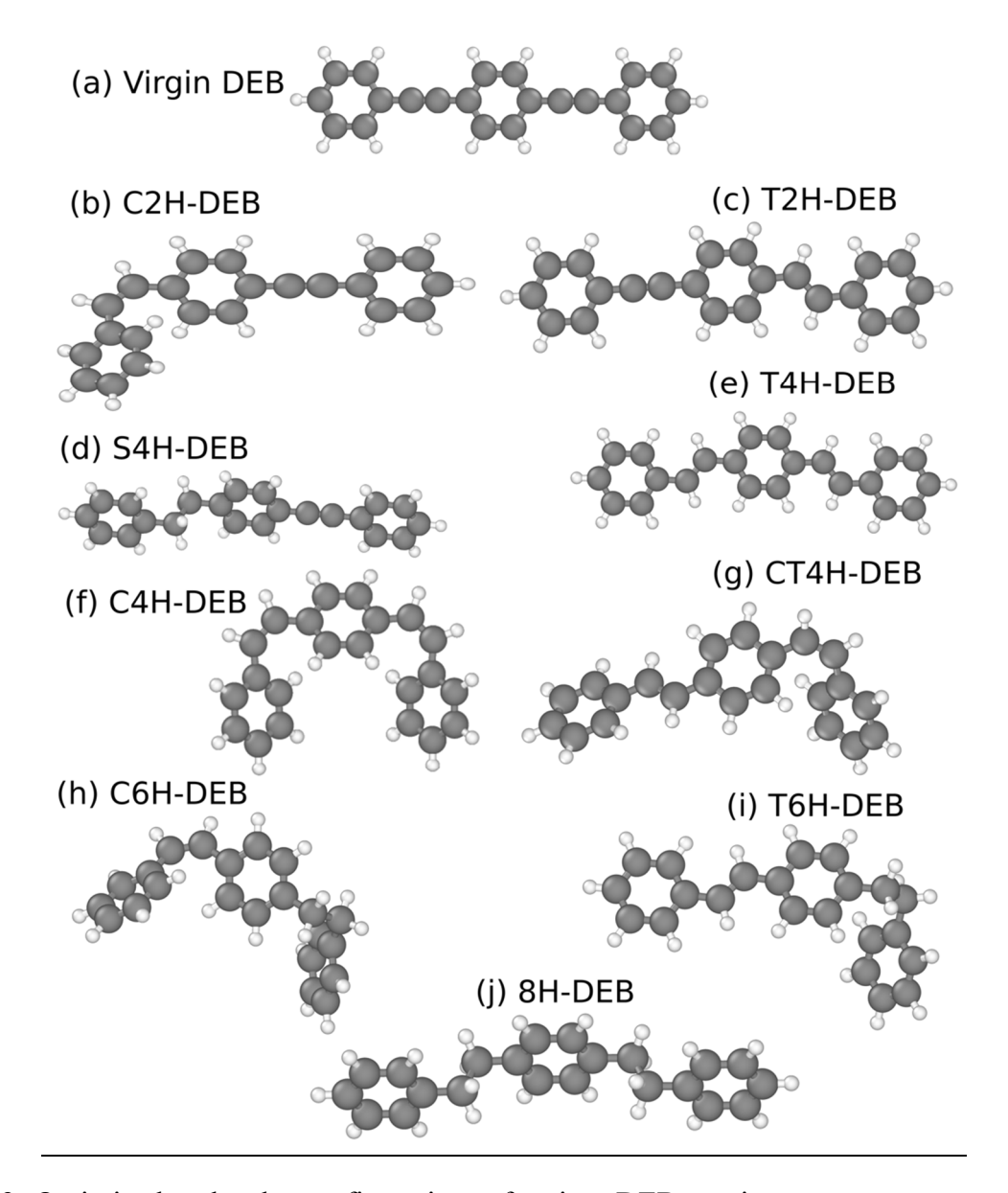


Figure 9: Optimized molecular configurations of various DEB species.

Relative energetics from the optimized DEB species are plotted in figure 10. Entropic contributions are assumed to be negligible for crystal stability and not considered here. This enthalpic representation shows that the hydrogenation reaction is highly favorable and exothermic (indicated by the negative values for the cumulative heat of formation, ΔE , at each hydrogenation step). The absolute values (hence positive numbers) of the heat of formation from successive

hydrogenation steps with reference to the preceding most stable hydrogenated states are labeled as "Rxn. Step $|\Delta E_i|$ " on the vertical axis of the inset in figure 10, and indicates the relative thermal stability of the hydrogenated DEB species in that step. Trans isomers resulting from each hydrogenated step are the most thermally stable isomers, followed by *cis-trans* isomers, and finally pure cis-cis isomers. Under suitable reaction conditions, the final hydrogenation product is expected to be the fully hydrogenated species (8H-DEB). The inset of figure 10 confirms the volatility order established by equilibrium vapor pressure and melting temperature measurements in the experimental section. As seen in figure 10, the difference in the heat of formation for each step in the hydrogenation process is in the range of 1-2 eV (in term of thermal energy, 1 eV ~ 11605K). The practical operating temperatures for these organic hydrogen getters are recommended to be below the melting point of the most volatile species (366.3K for 8H-DEB) to avoid excessive vaporization of materials and liquefaction which lead to contamination of adjacent materials. Since normal operating temperatures for these getters (< 366.3K) are equivalent to only a few percent of the 1-2 eV (~11605-23210 K) thermal energy needed to release hydrogen in any of the hydrogenation step, the hydrogen uptake by these getters is practically irreversible.

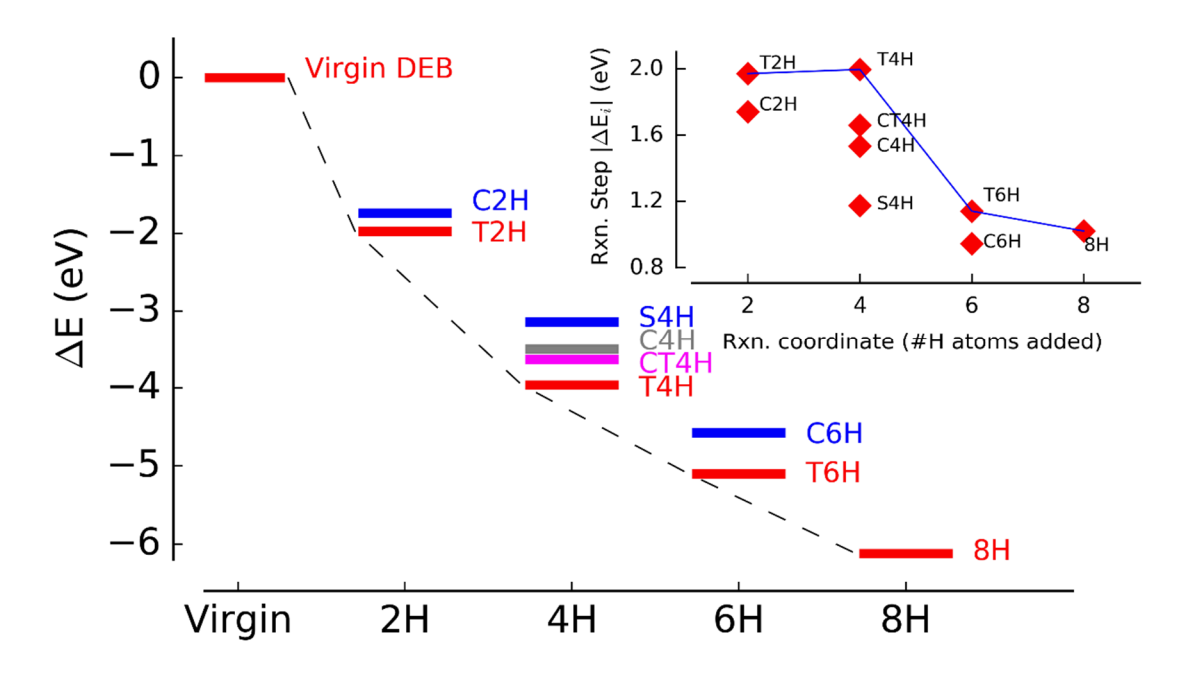


Figure 10: Relative thermodynamic stabilities of the DEB intermediates estimated from DFT calculations (the negative values for the cumulative heat of formation at each hydrogenation step imply favorable exothermic reactions). The absolute values (hence positive numbers) of the heat of formation from successive hydrogenation steps with reference to the preceding most stable hydrogenated states are labeled as "Rxn. Step $|\Delta E_i|$ " on the vertical axis of the inset, which shows that the formation of T4H-DEB is most favorable.

As discussed earlier, the collective CH bond dipole interactions in the crystal structures can play a significant role in the melting temperatures and equilibrium vapor pressures of these DEB species. Here, a computation to calculate the CH bond dipole moment in each DEB molecule was made. Atomic charge distribution in terms of electrostatic potential (ESP) are computed and dipole moment of each CH bond in the backbone was calculated using Eq. 6. Although the total dipole of a molecule (especially linear ones) is close to zero, the CH dipole moment are predicted

to be quite large (see Table 4). For the CH bond associated with a double bonded carbon, the dipole moment was computed to be ~0.7-0.8 D. This is mainly due to the concentration of electron density at the double bond, which creates a negative charge center around the carbon. CH bonds associated with single bonded carbons (mainly DEB species with 6 or more H added) showed much smaller dipole moments (~0.3-0.4 D). Computed bond dipole moment are in qualitative agreement with the experimental results and literature values. [25, 26]

Table 4: Computed molecular dipole moment (in Debye) and average CH bond dipole moment of DEB molecules using ESP charges from DFT. CH bond dipole for each DEB molecule is computed from atomic charge obtained via DFT and Eq. 6.

SN	Name	Total Dipole Moment (D) CH Bond Dipole Moment			
1	Virgin DEB	0.0	0.0		
2	T2H-DEB	0.2291	0.83		
3	C2H-DEB	0.4118	0.72		
4	T4H-DEB	0.0228	0.77		
5	S4H-DEB	0.2613	0.41		
6	C4H-DEB	0.3259	0.71		
7	T6H-DEB	0.4055	0.77ª		
			0.41 ^b		
8	C6H-DEB	0.4407	0.73 a		
			0.32 ^b		
9	8H-DEB	0.0134	0.43°		
			0.27 ^d		

- a. CH bond on sp2 carbon.
- b. CH bond on sp3 carbon.
- c. CH bond on sp3 carbon located on the outer side of the C-C backbone.
- d. CH bond on sp3 carbon located on the inner side of the C-C backbone.

The bulk crystal structures of virgin DEB (see figure 11, panels a1 and a2) and T4H-DEB (see figure 11, panels b1, b2, and b3) were optimized to obtain the ground state energy and corresponding lattice parameters. The parameters obtained here are in good agreement with the available literature information [27, 28] for both species. Lattice parameters and angles are reported in Table 5. Computed bulk densities were 0.99 g/cm³ and 1.03 g/cm³ for virgin DEB and T4H-DEB, respectively. Atomic coordinates of the bulk structures of virgin DEB and T4H-DEB are provided in the supporting information. Optimized crystal structures were used to predict the XRD pattern of virgin-DEB and T4H-DEB species. Experimental and model simulated XRD patterns simulated at Cu K α with $\lambda = 1.54056$ Å are shown in figure 11 (in panels c1 and c2). Overall, the simulated XRD peaks are in close agreement with experimental peaks. Some deviations are expected as the samples used in experiment may contain impurities and vacancies not present in perfect crystal. Panels d1-d3 (in figure 11) show the comparisons among IR peaks of virgin DEB obtained from experiment and simulations. As expected, simulated IR peaks from crystalline virgin DEB are in better agreement with the experimental peaks. In general, gas phase IR peaks are shifted to higher wavenumber.

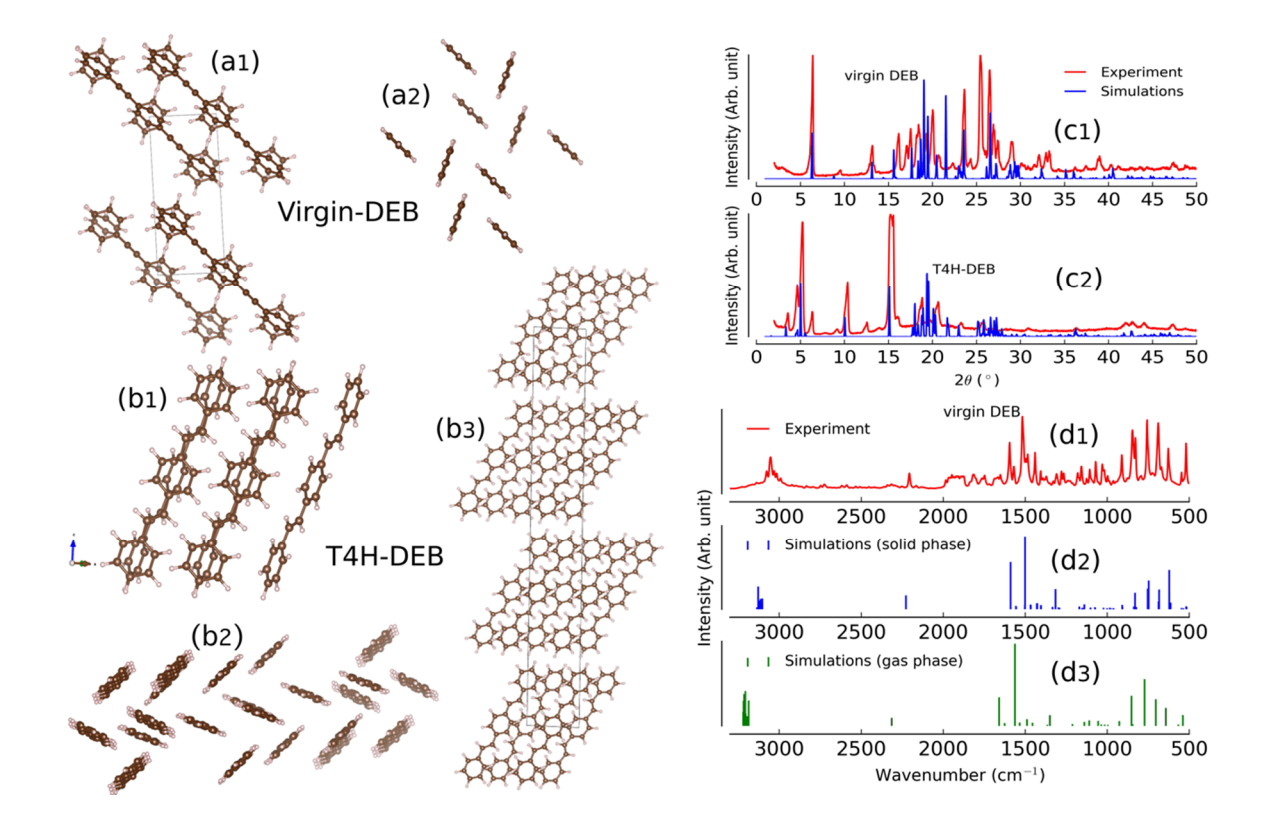


Figure 11: Crystal packing structures, experimental vs simulated XRD and IR peak comparisons of virgin-DEB and T4H-DEB. Panels a1 and a2: side view and top view of virgin DEB, panels b1, b2, and b3: side view, top view, and a unit cell (side view) of T4H-DEB, panel c1 and c2: Experimental and simulated XRD peak comparison of virgin-DEB and T4H DEB, panels d1, d2, and d3: experimental, simulated solid phase, and simulated gas phase IR peaks comparisons of virgin-DEB. Experimental XRD peaks are same as in figure 6. The XRD patterns were simulated at Cu Kα with $\lambda = 1.54056$ Å. A correction factor or 0.964 was applied for gas phase IR signals computed using B3LYP DFT functional set.

Table 5: Structural parameters of virgin and T4H-DEB from DFT optimization.

Name	Space group	Lattice parameter (in Å)		Lattice angle (in degree)			
		а	b	С	α	β	γ
Virgin	P1(triclinic)	5.99	9.57	13.70	90.91	95.03	104.38
DEB		$(6.0202)^{a}$	(9.662) ^a	(13.692) ^a	(90.719) ^a	(94.732) ^a	(103.859) ^a
T4H-	P1 (triclinic)	6.30	8.20	52.88	87.92	91.85	89.46
DEB		(5.91) ^b	(7.45) ^b	(51.92) ^b	(88.80) ^b	(89.64) ^b	(89.95) ^b

a. Parameters are from ref.[28]

Summary and Conclusions

In summary, the melting temperatures and equilibrium vapor pressures of virgin DEB, partially hydrogenated DEBs, and fully hydrogenated DEB getters have been assessed. A non-monotonic evolution of the volatility of the getter with increasing hydrogenation level was observed. *Trans* isomers resulting from each hydrogenated step are least volatile, followed by the *cis-trans* isomers, and finally pure *cis-cis* isomers. In all cases, species with a higher melting temperature also has a lower equilibrium vapor pressure. XRD analysis revealed the presence of T-shaped, sandwich type, and offset parallel type ring stacking in all DEB species. Quadrupole interaction, structural complexity, varying bond order, charge distribution, and packing alignment all have certain effects on the volatility of each DEB species. Nonetheless, collective CH bond dipole interactions in the various DEB crystal structures correspond well with the results from equilibrium vapor pressure and melting point experiments, and, therefore, play a significant role

b. Parameters are from ref.[27]

in the overall volatilities of the DEB series. These experimental results were confirmed by DFT calculations which also shed light on the thermodynamic favorability of the DEB hydrogenation reactions and energy molecular structures. The better than microTorr level equilibrium vapor pressures of the most volatile hydrogenated DEB product (8H-DEB) at temperatures as high as 353K suggest DEB can serve as a suitable hydrogen getter for gas-filled and high vacuum electronic applications with operational temperatures many tens of degrees above room temperature. The methodology described in this report can also be used analogously to determine the volatility trends and optimal operational temperatures for other catalytic hydrogenation processes as well.

Acknowledgement

This work was prepared by LLNL under Contract DE-AC52-07NA27344. Authors thanks Dr. S. C. McCall, Dr. W. J. Siekhaus, Dr. M. Kroonblawd, and Dr. R. Lindsey at LLNL for the helpful discussions.

ASSOCIATED CONTENT

Supporting Information. Comparison of melting points are shown in Table S1. Atomic coordinates of various DEB molecules are given in section S1.

References:

- 1. Galwey, A.K., *Solid state reaction kinetics, mechanisms and catalysis: a retrospective rational review.* Reaction Kinetics, Mechanisms and Catalysis, 2015. **114**(1): p. 1-29.
- 2. Schmalzried, H., *Solid-State Reactions*, in *Treatise on Solid State Chemistry: Volume 4 Reactivity of Solids*, N.B. Hannay, Editor. 1976, Springer US: Boston, MA. p. 233-279.

- 3. L'vov, B.V. and A.K. Galwey, *The mechanism and kinetics of NiO reduction by hydrogen.* Journal of Thermal Analysis and Calorimetry, 2012. **110**(2): p. 601-610.
- 4. Busca, G., *Preparation of Solid Catalysts: A Short Summary*, in *Heterogeneous Catalytic Materials*. 2014, Elsevier. p. 9--22.
- 5. Nigrey, P.J., *AN ISSUE PAPER ON THE USE OF HYDROGEN GETTERS IN TRANSPORTATION PACKAGING*, DOE, Editor. 2000, Sandia National Laboratory Albuquerque, NM.
- 6. Dinh, L.N., et al., *Hydrogen uptake of DPB getter pellets*. Journal of Nuclear Materials, 2008. **382**(1): p. 51-63.
- 7. Balooch, M., W.-E. Wang, and J.R. Kirkpatrick, *Hydrogen uptake mechanism of a silicone-rubber DEB getter mixture*. Polymer Physics, 2001. **39**(4).
- 8. Dinh, L.N., et al., *Aging aspects of DEB getters*. Journal of Nuclear Materials, 2013. **442**(1-3): p. 298-305.
- 9. Holtz, R.L., V. Provenzano, and M.A. Imam, *Overview of nanophase metals and alloys for gas sensors, getters, and hydrogen storage*. Nanostructured Materials, 1996. **7**(1): p. 259-264.
- 10. Powell, G.L., *Hydriding kinetics of an organic hydrogen getter-DPB*. Journal of Alloys and Compounds, 2007. **446**: p. 402-404.
- 11. Dinh, L.N., et al., Mechanism and Kinetic Modeling of Hydrogenation in the Organic Getter/Palladium Catalyst/Activated Carbon Systems. Journal of Physical Chemistry A, 2015. 119(6): p. 943-951.
- 12. Giorgi, T.A., B. Ferrario, and B. Storey, *An updated review of getters and gettering*. Journal of Vacuum Science & Technology A: Vacuum, Surfaces, and Films, 2016. **3**.
- 13. Smyrl, N.R. and G.L. Powell. Characterization of the Hydrogenation Products of Bis(phenylethynyl) Benzene (DEB) Getter Using Combined GC/FTIR/MS,FT-Raman, and ATR Spectroscopies. in ICAVS-6 Conference. 2011. Sonoma County, CA.
- 14. Stone, M., et al., *Improved Hydrogen Gas Getters for TRU Waste –Final Report*. 2005, Idaho National Laboratory: Idaho National Laboratory. p. 69.
- 15. Salazar, K.V., et al., *Hydrogen uptake on film surfaces produced by a unique codeposition process.* Applied Surface Science, 2003. **214**: p. 20-26.
- 16. Chemistry, R.S.o. http://www.chemspider.com/. 2017 [cited 2017 January 10].
- 17. Kresse, G. and J. Furthmuller, *Efficient iterative schemes for ab initio total-energy calculations using a plane-wave basis set.* Physical Review B, 1996. **54**(16): p. 11169-11186.
- 18. Frisch, M.J.T., G. W.; Schlegel, H. B.; Scuseria, G. E.; Robb, M. A.; Cheeseman, J. R.; Scalmani, G.; Barone, V.; Petersson, G. A.; Nakatsuji, H.; Li, X.; Caricato, M.; Marenich, A. V.; Bloino, J.; Janesko, B. G.; Gomperts, R.; Mennucci, B.; Hratchian, H. P.; Ortiz, J. V.; Izmaylov, A. F.; Sonnenberg, J. L.; Williams-Young, D.; Ding, F.; Lipparini, F.; Egidi, F.; Goings, J.; Peng, B.; Petrone, A.; Henderson, T.; Ranasinghe, D.; Zakrzewski, V. G.; Gao, J.; Rega, N.; Zheng, G.; Liang, W.; Hada, M.; Ehara, M.; Toyota, K.; Fukuda, R.; Hasegawa, J.; Ishida, M.; Nakajima, T.; Honda, Y.; Kitao, O.; Nakai, H.; Vreven, T.; Throssell, K.; Montgomery, J. A., Jr.; Peralta, J. E.; Ogliaro, F.; Bearpark, M. J.; Heyd, J. J.; Brothers, E. N.; Kudin, K. N.; Staroverov, V. N.; Keith, T. A.; Kobayashi, R.; Normand, J.; Raghavachari, K.; Rendell, A. P.; Burant, J. C.; Iyengar, S. S.; Tomasi, J.; Cossi, M.; Millam, J. M.; Klene, M.; Adamo, C.; Cammi, R.; Ochterski,

- J. W.; Martin, R. L.; Morokuma, K.; Farkas, O.; Foresman, J. B.; Fox, D. J., *Gaussian 09, Revision A.02*, 2016: Gaussian, Inc., Wallingford CT,.
- 19. Perdew, J.P., K. Burke, and M. Ernzerhof, *Generalized gradient approximation made simple*. Physical Review Letters, 1996. **77**(18): p. 3865-3868.
- 20. Becke, A.D., *Density-functional exchange-energy approximation with correct asymptotic behavior*. Phys Rev A Gen Phys, 1988. **38**(6): p. 3098-3100.
- 21. Lee, C., W. Yang, and R.G. Parr, *Development of the Colle-Salvetti correlation-energy formula into a functional of the electron density*. Phys Rev B Condens Matter, 1988. **37**(2): p. 785-789.
- 22. Stuart, B.H., *Infrared Spectroscopy: Fundamentals and Applications*. 2004: John Wiley & Sons.
- 23. Sinnokrot, M.O., E.F. Valeev, and C.D. Sherrill, *Estimates of the ab initio limit for pi-pi interactions: the benzene dimer.* J Am Chem Soc, 2002. **124**(36): p. 10887-93.
- 24. Battaglia, M.R., A.D. Buckingham, and J.H. Williams, *The electric quadrupole moments of benzene and hexafluorobenzene*. Chemical Physics Letters, 1981. **78**(3).
- 25. Hinchliffe, A. and I.F. Kidd, CH Bond Dipole. J.C.S. Faraday II, 1980. 76: p. 172-176.
- 26. Lazzeretti, P., R. Zanasi, and W. Raynes, *On the CH bond dipole moment in alkanes*. The Journal of Chemical Physics 1987. **87**: p. 1681-1684.
- 27. Varghese, S., et al., *Stimulated Emission Properties of Sterically Modified Distyrylbenzene-Based H-Aggregate Single Crystals.* J Phys Chem Lett, 2013. **4**(10): p. 1597-602.
- 28. Watt, S.W., et al., *Structure and phase behavior of a 2:1 complex between arene- and fluoroarene-based conjugated rigid rods*. Angew Chem Int Ed Engl, 2004. **43**(23): p. 3061-3.